PHILOSOPHICAL TRANSACTIONS OF THE ROYAL SOCIETY A MATHEMATICAL, PHYSICAL & ENGINEERING SCIENCES

Femtochemistry of the Reaction of IHgI: Theory Versus Experiment

M. Gruebele, G. Roberts and A. H. Zewail

Phil. Trans. R. Soc. Lond. A 1990 **332**, 223-243
doi: 10.1098/rsta.1990.0111

Femtochemistry of the reaction of IHgI: theory versus experiment

By M. Gruebele, G. Roberts and A. H. Zewail

Arthur Amos Noyes Laboratory of Chemical Physics, California Institute of Technology, Pasadena, California 91125, U.S.A.

Recently, the rapid dissociation dynamics of mercury diiodide has been studied by femtosecond transition-state spectroscopy (FTS). Such experiments provide a real-time picture of wave packet motions in two dissociation channels associated with the iodine atomic product in its ground and spin–orbit excited states. We present here a two-dimensional quantum mechanical treatment of the FTS experiment, which allows us to discuss the salient features of the wave packet motion and product state distribution. Possible refinements of the approach and their significance are also discussed.

1. Introduction

Progress has been made in developing femtosecond transition-state spectroscopy (FTS) and its applications to the direct real-time study of ultrafast elementary chemical reactions (Zewail 1988; Zewail & Bernstein 1988; Gruebele & Zewail 1990; Khundkar & Zewail 1990). In FTS, a first femtosecond laser pulse promotes a precursor molecule to a dissociative state of interest, thus establishing the zero-of-time of the reaction. From there, the molecular wave packet propagates on the excited state potential energy surface (PES), leading to product fragments. Before reaching the asymptotic limit, the wave packet is probed by a second femtosecond laser pulse at different wavelengths, imaging its motion as various scalar and vector (alignment) dynamical effects (Dantus *et al.* 1989*a*; Zewail 1989) develop from reagent to products.

The technique has been used to study a number of reactions with different types of PESs. The dissociation of ICN to I and CN involves a repulsive potential curve, featuring a single transient or a build-up in the FTS signal, depending on whether the transitory or asymptotic region of the reaction is being probed (Scherer *et al.* 1985; Dantus *et al.* 1987, 1988). The dissociation of NaI occurs via an avoided crossing from a quasi-bound state into the continuum, resulting in an oscillatory FTS transient due to vibrational motion of the wave packet as it leaks to atomic products (Rosker *et al.* 1988*a*; Rose *et al.* 1988, 1989). Molecular iodine has been studied in the bound $B^3\Pi_{0^+u}$ electronic state (Bowman *et al.* 1989*a*; Dantus *et al.* 1990), in which vibrational and rotational motions are revealed with sufficient accuracy to allow a determination of its potential curve from purely temporal data (Gruebele *et al.* 1990). Dissociative states of iodine have also been studied (Bowman *et al.* 1989*a*).

Although these processes potentially involve several vibrational and rotational motions, their fundamental characteristics can be reduced to a one-dimensional

Phil Trans R. Soc. Lond. A (1990) **332**, 223–243 *Printed in Great Britain*

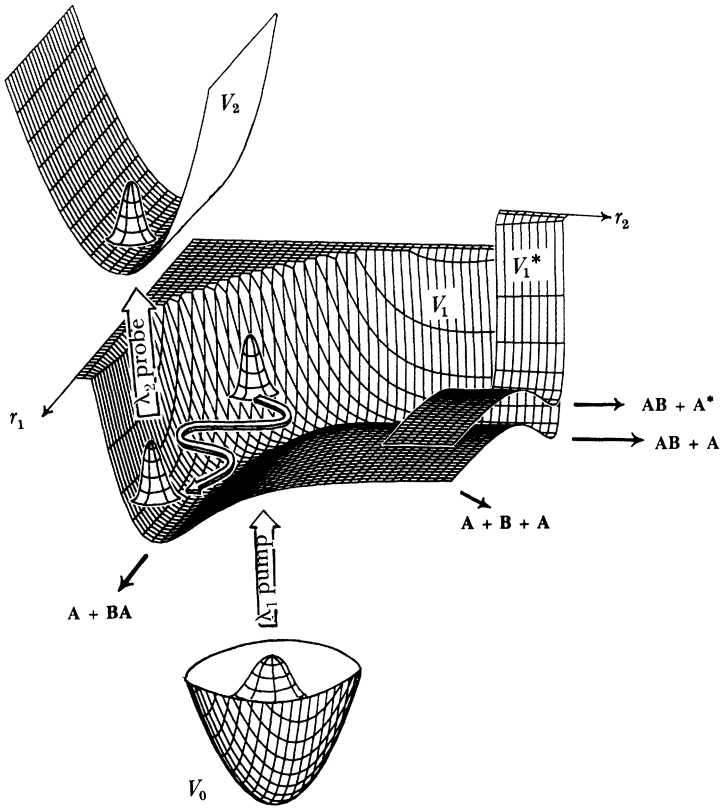

Figure 1. General two-dimensional FTS experiment. The ground state wave function is pumped from V_0 to V_1 (or a spin–orbit excited V_1^*, as in the case of HgI_2). After propagating for a time τ (only one channel shown schematically for simplicity), it is probed at λ_2 to surface V_2, from where it is detected by LIF or another suitable procedure. The time-resolved probing images the motion of the packet on V_1.

problem. Such is not the case with the reaction of HgI_2, which has recently been studied in this group (Bowman *et al.* 1989*b*; Dantus *et al.* 1989*b*). Depending on the energy of excitation, several channels are open to dissociation:

$$\begin{aligned} \mathrm{IHgI}^* &\rightarrow [\mathrm{I}\ldots\mathrm{Hg}\ldots\mathrm{I}]^{\ddagger *} \rightarrow \mathrm{Hg}\,(^1\mathrm{S}_0) + \mathrm{I} + \mathrm{I} \\ &\rightarrow [\mathrm{I}\ldots\mathrm{Hg}\ldots\mathrm{I}]^{\ddagger *} \rightarrow \mathrm{HgI}\,(\mathrm{X}^2\Sigma^+) + \mathrm{I}\,(^2\mathrm{P}_{\frac{3}{2}}) \text{ or } \mathrm{I}(^2\mathrm{P}_{\frac{1}{2}}). \end{aligned} \tag{1}$$

The separating fragments leave an image of their vibrational and translational motions in the oscillatory behaviour of the FTS signals. In this case, the pump laser prepares a wave packet near the saddle point of the excited state PES, whence it proceeds in a motion that involves intimate coupling of the symmetric and antisymmetric stretching coordinates (figure 1). Furthermore, there are interactions with the bending vibration and rotational angular momentum, and conical intersections of electronic surfaces. It is clear, however, that the simplest quantitative explanation of the experimental observations must involve consideration of the two stretching vibrational degrees of freedom, which are the most important at early times. This reaction thus provides an opportunity to study the scalar and vector

dynamics in a system of well-defined dimensionality. Because the fragment HgI is produced hot, it is also possible to distinguish different local areas in the wave packet that lead to different rotational and vibrational states of the final products.

Besides the recent FTS studies, there is a wealth of information available in the literature on the HgI_2 system (Wilcomb *et al.* 1976*a*, *b*; Mayer *et al.* 1977*a*, *b*; Hofmann & Leone 1978; McGarvey *et al.* 1981; Oprysko *et al.* 1983). Hofmann & Leone (1978) have studied the energy-dependent quantum yields of $I(^2P_{\frac{3}{2}})$ and $I^*(^2P_{\frac{1}{2}})$ atoms. McGarvey *et al.* (1981) investigated dissociation to, and emission from, HgI fragments in the $B^2\Sigma^+$ state. Bernstein and co-workers have studied the $Hg+I_2$ reactive system by crossed beams (Wilcomb *et al.* 1976*a*, *b*; Mayer *et al.* 1977*a*; Oprysko *et al.* 1983) from which they were able to determine the ground state PES (Mayer *et al.* 1977*b*). A number of studies have elucidated the spectroscopy of the HgI fragment in both its $X^2\Sigma^+$ and $B^{2+}\Sigma^+$ states (Wieland 1929, 1960; Wilcomb & Bernstein 1976; Cheung & Cool 1979; McGarvey *et al.* 1981; Tellinghuisen *et al.* 1982; Viswanathan & Tellinghuisen 1983; Salter *et al.* 1986; Dreiling & Setser 1987; Zhang *et al.* 1987; Bhartiya *et al.* 1990), providing a benchmark for the asymptotic behaviour of the reaction. In addition, investigations of mercury dihalide spectra beginning in 1927 (Terenin 1927; Wieland 1929, 1932; Butkow 1931; Wehrli 1938; 1940; Sponer & Teller 1941; Maya 1977, 1978; Husain *et al.* 1980; Wilcomb *et al.* 1980; McGarvey *et al.* 1981; Cheung *et al.* 1982; Whitehurst & King 1987), radiative lifetimes (Hutchinson & Theocharous 1981), absorption cross-sections (Maya 1977; Hofmann & Leone 1978; Wilcomb *et al.* 1980), and theoretical studies (Wadt 1979, 1980) provide a fertile ground for analysis.

In a previous publication (Dantus *et al.* 1989*b*) we have analysed the HgI_2 FTS data in terms of two-dimensional quasiclassical trajectory calculations. These could not generate the observed FTS transients, but gave good agreement with the HgI fragment emission spectra (probed to the $B^2\Sigma^+$ state) and reaction time. In this paper we present a fully quantum mechanical treatment of the FTS dissociation experiments in the form of a two-dimensional wave packet propagation model problem and calculations of the HgI fragment spectroscopy. The remainder of this paper considers the main experimental results (§2), followed by an outline of the theoretical framework and calculational method (§3), and a detailed discussion of the results of HgI_2 (PES and dynamics) in the light of experiments and previous classical simulations (§4).

2. Summary of experimental results

Here we outline the results necessary for an analysis of the HgI_2 femtochemistry. As a guide, figure 1 shows the wave packet motions for a general ABA triatomic collinear dissociation. For the more technical details of the HgI_2 FTS experiments, the reader should consult the paper of Dantus *et al.* (1989*b*).

Ground state HgI_2 was excited by a laser pulse at $\lambda_1 = 310$ nm. This amounts to about 1350 cm^{-1} of energy available for total dissociation to mercury and two iodine atoms via the I* channel, and about 8950 cm^{-1} for the I channel (including thermal and zero-point energy of the stretching modes). As the HgI and I/I* (or Hg+2I) fragments separate, they are probed by a second laser pulse at $\lambda_2 = 620$ or 390 nm. At short interfragment distances, the separation between the PESs leading to HgI product in its $X^2\Sigma^+$ and $B^2\Sigma^+$ states is smaller than in the asymptotic limit. The 620 nm pulse thus probes early times, and 390 nm the long-time behaviour of the reaction. Correspondingly, at 620 nm, with detection of the fluorescence using a

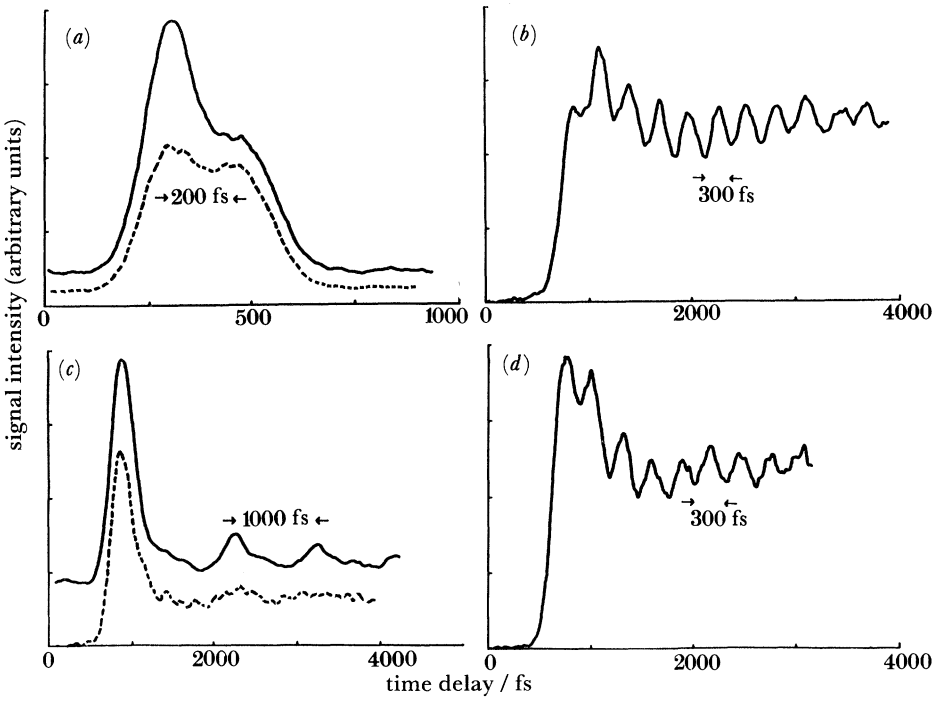

Figure 2. Experimental FTS transients at a pump wavelength (λ_1) of 310 nm. (*a*) displays transient behaviour at $\lambda_2 = 620$ nm, probing the early-time passage of the wave packet through the transition region; the I* peak lags the earlier I channel peak by about 200 fs (—, ⊥; – – –, ∥). (*b*), (*c*) and (*d*) show asymptotic probing of the wave packet at 390 nm, at detection wavelengths sensitive to either (*b*) the I* (427.5 nm) or I channels (*c*) (—, 360 nm; – – –, 432.5 nm), or (*d*) both (440 nm), with a corresponding difference in vibrational excitation and intensity of the initial 'full dissociation' peak.

monochromator at various wavelengths λ_{det}, a single slow peak (corresponding to the I* channel) and a single fast peak (corresponding to the I channel) are observed (Bowman *et al.* 1989*b*; Dantus *et al.* 1989*b*) as displayed in figure 2*a*, corresponding to the wave packets moving briefly through an absorption-resonant region.

Figure 2*b–d* shows four transients probed at 390 nm, differing only in the detection wavelength λ_{det}. They are of very dissimilar characteristics, even when detected at nearby wavelengths (e.g. $\lambda_{det} = 427.5$ and 432.5 nm). Figure 2*b* shows rapid oscillations (with a period of 300 fs at longer times) at $\lambda_{det} = 427.5$ nm, corresponding to HgI vibrational motion near the bottom of the anharmonic potential well, whilst figure 2*c* shows an initial sharp peak followed by slow oscillations (with a period of about 1 ps), corresponding to highly excited vibrational motion of HgI near the dissociation limit. The slow period dominates at both $\lambda_{det} = 360$ nm and 432.5 nm. At still other detection wavelengths (e.g. 440 nm in figure 2*d*), a superposition of these features can be observed.

This can be explained in terms of the sensitivity of the emission spectrum of HgI to the vibrational product distribution (Dantus *et al.* 1989*b*). In the I* channel, relatively little energy is available for vibrational and translational excitation, having mostly been taken up by spin-orbit excitation of I atoms. Ground state $HgI(X^2\Sigma^+)$ is formed in low vibrational levels, then probed to the $B^2\Sigma^+$ state. The resulting levels fluoresce strongly at 427.5 nm, less at 440 nm, and very little at 432.5

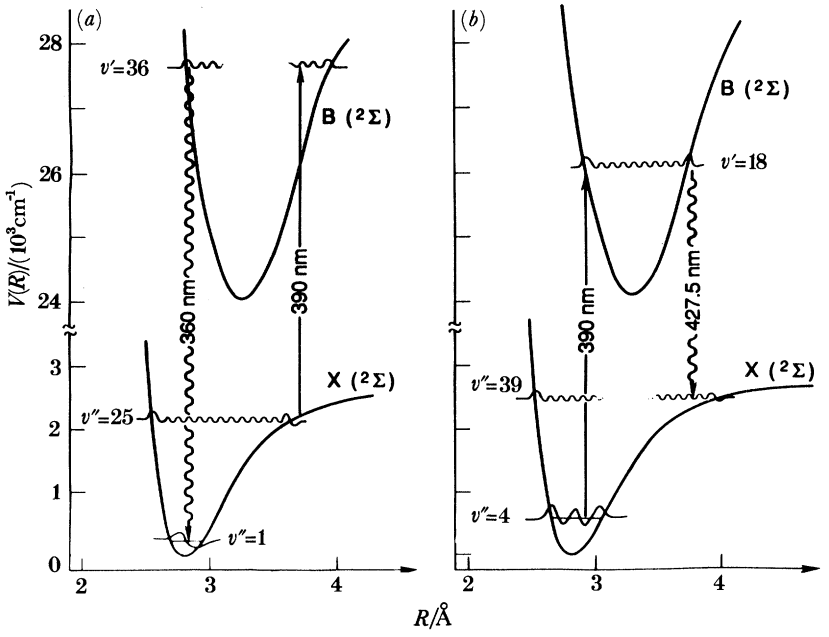

Figure 3. The Franck–Condon overlap between the $X^2\Sigma^+$ and $B^2\Sigma^+$ potential functions results in wavelength-selective LIF detection of vibrational product excitation in FTS experiments. (*a*) shows how high vibrational excitation of the product ($v'' = 25$) leads to emission at 360 nm (and also at 432.5 nm, not shown here); (*b*) shows how low vibrational excitation ($v'' = 4$) leads to emission at 427.5 nm.

or 360 nm compared to the I channel. In the I channel, highly vibrationally excited $X^{2+}\Sigma^+$ product is formed and probed to a different set of $B^2\Sigma^+$ state vibrational levels; these fluoresce strongly at 432.5 and 360 nm, less at 440 nm, and little at 427.5 nm, relative to the I* channel. These fluorescence spectrum thus allows a selection of the dynamics to be probed (figure 3).

The above analysis was verified in our earlier work (Dantus *et al.* 1989*b*) by a two-dimensional classical trajectory calculation, which yielded dissociation times and vibrational distributions in good agreement with experiment. The following quantum simulation of the HgI_2 dissociation allows a more detailed comparison with the FTS transients, as well as pointing to a number of interesting features of the reaction dynamics and PES.

3. Theory

A number of theoretical approaches have been devised over the past years to account for the time-resolved features observed in FTS experiments. Numerous classical (Bersohn & Zewail 1988; Dantus *et al.* 1988; Rosker *et al.* 1988*b*; Benjamin & Wilson 1989; Bernstein & Zewail 1989; Lee *et al.* 1989*a*; Rose *et al.* 1989), semiclassical (Marcus 1988), and quantum (Williams & Imre 1988*a*, *b*; Engel *et al.* 1988, 1990; Choi & Light 1989; Engel & Metiu 1989*a*, *b*, *c*, 1990; Heather & Metiu 1989; Imre & Zhang 1989; Lee *et al.* 1989*b*, *c*; Lin & Fain 1989; Yan *et al.* 1989) calculations have been done on the one-dimensional systems mentioned earlier (with or without inclusion of rotations) and related systems (Kono & Fujimura 1989; Yamashita & Morokuma 1989).

PHILOSOPHICAL TRANSACTIONS OF THE ROYAL SOCIETY A MATHEMATICAL, PHYSICAL & ENGINEERING SCIENCES

Realistic quantum dynamical calculations for few-dimensional systems have become feasible recently due to conceptual and computational advances. The formalism for wave packet analysis of spectral and temporal features of dissociation reactions was first devised by Heller and co-workers (Heller 1975, 1981; Huber & Heller 1987; Henriksen & Heller 1989). The subsequent development of fast propagator algorithms by Feit and co-workers (Fleck *et al.* 1976; Feit *et al.* 1982, 1983) and Kosloff & Kosloff (Kosloff & Kosloff 1983*a*, *b*; Kosloff 1988) made quantum dynamical calculations on small systems possible, although speed and storage requirements still limit calculations to three or fewer dimensions. The earliest detailed quantum mechanical studies of FTS reaction dynamics were made by Williams & Imre (1988*a*, *b*) and Metiu and co-workers (Engel *et al.* 1988, 1990; Engel & Metiu 1989*a*, *b*, *c*, 1990; Heather & Metiu 1989). In the following two subsections, we present our formalism and computational implementation, focusing on features of the HgI_2 dissociation reaction.

(*a*) *Formalism*

Figure 1 shows a schematic FTS experiment in two dimensions for a triatomic molecule with collinear bonds. The pump laser (λ_1) excites the ground-state wavefunction from surface V_0 to surface V_1. There, a superposition of eigenstates (discrete or continuum, or both) at energies E_{1i} is formed. The energy spread of the resulting wave packet depends on the spectral width $g(E)$ of the laser pulse. The wave packet then propagates on V_1, acquiring the characteristics of the products while approaching the asymptotic region of the PES. After a time delay τ, it is probed by a second laser pulse (λ_2^*) to surface V_2. From there, the excited transitional species can be detected by emission back to surface V_1. The separation of the surface V_1 and V_2 varies along the reaction coordinate, so the wave packet can be probed at specific spatial positions by tuning the probe pulse wavelength. Furthermore, the dispersed emission is sensitive to the energy level populations, and can be used to study selectively certain spectral regions of surface V_1.

If the pump and probe pulses are sufficiently well-spaced in time, the two processes can be regarded separately. In the weak-field dipole approximation, the spectral picture for the final wave packet on V_2 before emission is ($\hbar = 1$ for simplicity)

$$\Psi(t) = \sum_{1i,\,2\alpha} |2\alpha\rangle \, \mathrm{e}^{-\mathrm{i}E_{2\alpha}t} g_{1i,\,2\alpha} \langle 2\alpha|\mu_{1,\,2}(\boldsymbol{r})\,|1i\rangle \, \mathrm{e}^{-\mathrm{i}E_{1i}\tau} g_{0,\,1i} \langle 1i|\mu_{0,\,1}(\boldsymbol{r})|0\rangle, \tag{2}$$

where $g_{0,1}$ and $g_{1,2}$ are the spectral lineshapes of the laser electric field E_L, with a maximum at $g(0)$; in all that follows, we assume the gaussian form

$$g_{1i,\,2\alpha} = E_L \exp\left[-(E_{2\alpha} - E_{1i} - \omega_{1,\,2})^2/\sigma_E^2\right]. \tag{3}$$

$\mu_{0,1}(\boldsymbol{r})$ and $\mu_{1,2}(\boldsymbol{r})$ are the transition dipole operators, E_{1i} and $E_{2\alpha}$ are eigenstate energies on surfaces V_1 and V_2, and $\omega_{1,2}$ is the central frequency of the probe pulse (corresponding to λ_2 in figure 1). Inserting complete sets of states, this simplifies to

$$\Psi(t) = \mathrm{e}^{-\mathrm{i}H_2 t - \tau} g_{1,\,2}(H_2 - H_1 - \omega_{1,\,2})\,\mu_{1,\,2}(\boldsymbol{r})\,\mathrm{e}^{-\mathrm{i}H_1\tau} g_{0,\,1}(H_1 - H_0 - \omega_{0,\,1})\,\mu_{0,\,1}(\boldsymbol{r})\,\Psi_0, \tag{4}$$

where H_1 and H_2 are the hamiltonian operators on surfaces V_1 and V_2, and $\omega_{0,1}$ is the central frequency of the pump pulse (corresponding to λ_1 in figure 1). Unfortunately, the action of the line-shape operators g (defined in analogy to equation (3)) on the

wavefunction is difficult to evaluate, particularly for continuum states in more than one-dimensional systems, where basis set methods are rather ineffective, and for long light pulses, where perturbation expansions such as

$$e^{-H^2/\sigma_E^2}\mu\Psi \sim \mu\Psi-(H^2/\sigma_E^2)\,\mu\Psi+\ldots, \tag{5}$$

fail to converge.

This can be alleviated by Fourier transforming equation (2) into a fully temporal, rather than spectral guise (Loudon 1973). By decomposing the laser pulse into small slices Δt (maintaining their coherent relation), the perturbation method can be made to converge for each slice. At the first-order level, we need only use the first term in equation (5), i.e. an exact copy of $\mu\Psi$ is promoted, and both promoted and original wavefunctions then propagate on their respective surfaces. In the limit $\Delta t\to 0$, this simply yields the first-order time-dependent perturbation theory version of equation (2),

$$\Psi(t) = T_2(t-\tau)\,U_{1,2}\,T_1(\tau)\,U_{0,1}\,\Psi_0, \tag{6a}$$

where, from right to left, the ground-state wavefunction is pumped to surface V_1 by operator $U_{0,1}$, propagates for time τ, is probed to surface V_2 by operator $u_{1,2}$, and continues to propagate to a final time t. The final wavefunction is not normalized to unity.

In practice, the first-order perturbation operators must be truncated at a finite time to prevent the light pulses from overlapping, and we use a more specific form of equation (6*a*),

$$\Psi(t) = T_2(t-\tau-2\sigma_t)\,U_{1,2}(4\sigma_t)\,T_1(\tau-4\sigma_t)\,U_{0,1}(4\sigma_t)\,\Psi_0, \tag{6b}$$

with the explicit operators given by

$$T_0(t) = e^{-iH_0t}, \quad T_1(t) = e^{-i(H_1-\omega_{0,1})t}, \quad T_2(t) = e^{-i(H_2-\omega_{0,1}-\omega_{1,2})t},$$

$$U_{0,1}(4\sigma_t)\,\Psi = \int_{-2\sigma_t}^{2\sigma_t} dt'\,T_1(2\sigma_t-t')\,\mu_{0,1}\,g'_{0,1}\,T_0(t')\,\Psi(t'), \tag{7}$$

with an analogous formula for $U_{1,2}$. $g'(t)$ is the temporal laser lineshape.

$$g'(t) = E'_L \exp[-(t-t_0)^2/\sigma_t^2], \tag{8}$$

taken to be gaussian, of the Fourier transform limited pulse g. In equations (6) and (7), the pulses are arbitrarily truncated at ± 2 standard deviations, and the operators U promote the wavefunction over a time period $4\sigma_t$, thereby shortening the period over which the time propagators T are applied in equation (6*b*). The wave packet is thus propagated from time $-2\sigma_t$ to time t in equation (6*b*), and promoted by pulses separated by at least $4\sigma_t$ in time.

Considering a single laser-molecule interaction in equation (7), in the limit where $g'(t)\to\delta(t)$ and the absorption spectrum is broad, the promoted wavefunction is a nearly exact copy of the original wavefunction, since a complete set of excited states is accessible to produce a faithful representation; in the limit where $\sigma_t\to\infty$, and $g'(t)$ is a constant, the promoted packet collapses to an eigenfunction on resonance, or has no amplitude off resonance.

Since time-integrated emission from V_2 to V_1 is detected, the coherence characteristics of the wave packet on surface V_2 do not contribute to the signal. Rather, only the wave packet motion on surface V_1, 'photographed' at various intervals t, contributes coherently to the experimentally observed signal. In

analysing emission spectra, with a lifetime $t_{\text{emission}} \gg t_{\text{reaction}}$, one can thus neglect the coherence of the eigenstates in the final wave packet, and concentrate on the relative populations of the energy levels instead. If only the total emission intensity is desired, the overall population $\langle \Psi(t)\Psi(t) \rangle$ immediately after the probe pulse yields the desired result, if there are no competing processes.

(*b*) *Calculations*

The wave packets were propagated using the split-operator method developed by Feit *et al.* (Fleck *et al.* 1976; Feit *et al.* 1982, 1983), amended to allow the kinetic energy to be a general quadratic form. Its speed and accuracy result from the third-order (in time) propagator expression

$$\Psi(t+\Delta t) = \mathrm{e}^{-\frac{1}{2}\mathrm{i}T\Delta t}\,\mathrm{e}^{-\mathrm{i}V(r)\Delta t}\,\mathrm{e}^{-\frac{1}{2}\mathrm{i}T\Delta t}\,\Psi(t), \tag{9}$$

discretized on a grid (T is the kinetic energy operator), with the wave function switched between the momentum and position representations by fast Fourier transform (FFT) and propagated by simple phase shifts between FFTs. The method has the advantage that the time step size required for convergence depends only on the characteristic energy spread ΔE of the problem, not an absolute energy scale (i.e. $\langle \Psi | H | \Psi \rangle^2 - \langle \Psi | H^2 | \Psi \rangle$ must be small, but not $\langle \Psi | H | \Psi \rangle$). In our calculations ΔE is approximately equal to the laser spectral bandwidth. Collinear two-dimensional calculations were carried out using the hamiltonian operator

$$H = \frac{1}{2\mu}(p_2^1 + p_2^2) - \frac{1}{2m_{\mathrm{B}}} p_1 p_2 + V(r_1, r_2), \tag{10}$$

where V is the desired potential, r_1 and r_2 are the two bond lengths of the symmetric triatomic ABA, and μ is the AB reduced mass. Since the problem is symmetrical, we will henceforth consider the region $r_1 > r_2$, such that r_1 becomes the reaction coordinate, and $r_2 = R$ the HgI product stretching coordinate at large separations (i.e. that part of the full wave packet shown in figure 1 will be considered). Our calculations of HgI_2 were carried out over bond distances ranging from 2–7 Å† or 2–12 Å, depending on the time and distance required to achieve near-asymptotic behaviour. The grid size ranged from 256×256 to 1024×1024 points, depending on the wave packet energy and distance range. The main considerations were sampling above the Nyquist limit (Feit *et al.* 1982, 1983) in momentum space for momentum wave functions, and in position space for all HgI bound states up to $v'' = 43$, to avoid aliasing and edge effects due to insufficient sampling of the discretized wave function. Convergence was also monitored as a function of the time step, with satisfactory results generally obtained for $\Delta t < 1/(50\Delta E)$ over the 200–1000 fs propagation period.

Whereas most calculations were carried out using gaussian wave packets on the excited dissociative PES (see §4 (*b*)), calculations were also done using the time-slice approximation (discretized equation (6)) to test the effect of pumping. Each time step Δt in these calculations consists of adding the modified ground state wave function $\mu\Psi$ to the upper state wavefunction, and propagating both simultaneously by a time Δt using the split-operator technique. The time step may be considerably smaller than for propagation, since the characteristic energy scale can be very large in the off-resonant case.

† 1 Å $= 10^{-10}$ m $= 10^{-1}$ nm.

PHILOSOPHICAL TRANSACTIONS OF THE ROYAL SOCIETY A MATHEMATICAL, PHYSICAL & ENGINEERING SCIENCES

In many cases, the asymptotic problem can be reduced to one dimension, namely that of the HgI stretching coordinate. While the problem is strictly only separable for product wave packets $\Psi(r_1)\,\Psi(r_2)$, the increasing loss of features of the translational projection of the wave function results means that sections parallel to $R = r_2$ (HgI stretch) at various r_1 (translational positions) in the asymptotic region can be used to characterize with reasonable accuracy vibrational coherence and distributions of the products. The momentum flow fronts are approximately parallel to r_1, resulting in little communication between different translational slices of the wave function. This allows one to project sections of the full wave packet onto HgI eigenstates at selected values of r_1,

$$\Psi_{\text{bound}}(r_1 = \text{const.}, r_2 = R, t) = \sum_i |\Psi_i(R)\rangle \langle \Psi_i(R)|\Psi_{\text{HgI}_2}(r_1, r_2 = R, t)\rangle, \qquad (11)$$

where Ψ_i is the ith vibrational wave function of HgI($X^2\Sigma^+$). To that effect, the modified Numerov algorithm of Johnson (1977) has been used to compute eigenfunctions in the $X^2\Sigma^+$ and $B^2\Sigma^+$ states of HgI. For the $X^2\Sigma^+$ state, a converged set of bound states from $v'' = 0$–43 has been calculated using 1001 grid points over the range 2.3–7.0 Å, as well as a sampling of continuum wave functions (for bound to continuum B–X emission calculations). For the $B^2\Sigma^+$ state, all vibrational states ($v' = 14$–40) with sizeable Franck–Condon factors have been evaluated; the resulting Franck–Condon factors are in good agreement with experimental results (Cheung & Cool 1979). These can then be used in calculating long time (greater than 300 fs) FTS transients, population distributions, and emission spectra.

4. Results for IHgI Reaction

(*a*) *The* PES

The large masses of mercury and iodine have so far precluded a detailed *ab initio* study of the ground and excited states PES. We must thus resort to simple model potentials which can be adjusted to reflect the most important features of the experiments.

The PES poses two problems that cannot be fully resolved by the present calculations: the importance of the bending motion and the possibility of (multiple) conical intersections. Relativistic *ab initio* calculations by Wadt (1979, 1980) confirm expectations from Walsh diagrams, indicating that the excited states of $HgCl_2$ and $HgBr_2$ are bent. From figure 1, it is evident that the initial motion of the wave packet will be outward along the symmetric stretching coordinate. In addition, there will be a motion along the bending coordinate, which will manifest itself as rotational excitation of the HgI fragment and alignment anisotropy. However, as seen from the experiments of Bowman *et al.* (1989*b*) and Dantus *et al.* (1989*b*) and the calculations shown below, the reaction is essentially complete (within 400 fs) in less than a single bending vibrational period (probably close to the ground-state bending vibrational period of *ca.* 1 ps (Sponer & Teller 1941)). This separation of bending and stretching (reaction) timescales allows the most important features of the experiments to emerge from a two-dimensional treatment alone, although at high vibrational energies the stretching motion may have a comparable frequency with the bend due to anharmonicity.

The photolysis experiments of Hofmann & Leone (1978) can be discussed in terms of excitation of the I* channel surface alone, followed by partial Landau–Zener

PHILOSOPHICAL TRANSACTIONS OF THE ROYAL SOCIETY A MATHEMATICAL, PHYSICAL & ENGINEERING SCIENCES

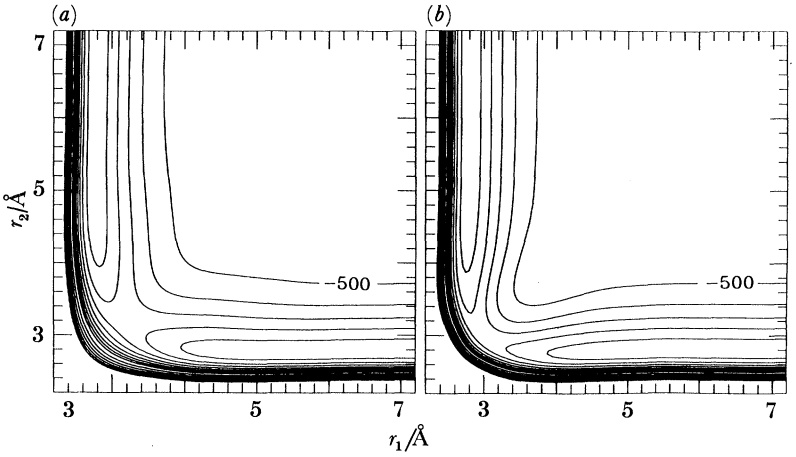

Figure 4. The two PESS used in most of the present calculations. (*a*) corresponds to a wide-channel surface, and was also used in previous classical trajectory calculations (Dantus *et al.* 1989*b*); (*b*) corresponds to a narrower-channel surface.

crossing at a conical intersection with the I surface, or in terms of separate excitation to the I and I* surfaces. The I* cross-section peaks at about 4300 cm^{-1} higher photolysis energy than the I cross-section, which could be due to the higher fragment velocity required for crossing between the two adiabatic surfaces, or the decreased spin–orbit splitting of the two approaching surfaces at small bond distances.

This ambiguity has not been completely resolved experimentally at the present time, but available FTS experiments suggest the crossing may occur at distances less than the HgI_2 equilibrium geometry. In the experiments of Dantus *et al.* (1989*a*, *b*), the I* channel transients probed at $\lambda_2 = 390$ nm correspond to a parallel transition; the polarization of the I channel transients at the same probe wavefunction has not yet been analysed due to the presence of a strong initial peak (arising from dissociation to Hg+2I), thus far preventing the assignment of the transition as parallel or perpendicular. However, the intensity ratio of the I channel peak to I* channel peak of the $\lambda_2 = 620$ nm transients is greater for perpendicular than parallel detection (figure 2*a*) at all detection wavelengths, suggestive of a perpendicular I channel transition. Thus, we consider the case of the crossing point lying at less than 2.61 Å (ground state equilibrium bond length (Allen & Sutton 1950)), with two independent surfaces. While this gives agreement with the most important experimental features, it should not be taken to exclude the possibility of an important role for surface crossings in the dissociation of IHgI, which, as discussed above, could emerge from a future more complete anisotropy analysis of transients at several pump energies.

We used a damped Morse oscillator excited state PES identical to that used for the classical trajectory calculations (Dantus *et al.* 1989). The explicit form is given by

$$V(r_1, r_2) = D\left[1-\exp\left\{-\beta\frac{e^{-\gamma r_1}(r_1-r_e)/r_e + e^{-\gamma r_2}(r_2-r_e)/r_e}{e^{-\gamma r_1}+e^{-\gamma r_2}}\right\}\right]^2 - D, \qquad (12)$$

where the parameters D, β, and r_e are allowed to vary according to

$$f = f_0 + f_1 \exp\left[-(r_1-r_2)^2/\sigma_f^2 - (r_1+r_2-2r_e)^2/\sigma_{f+}^2\right]. \qquad (13)$$

PHILOSOPHICAL TRANSACTIONS OF THE ROYAL SOCIETY A MATHEMATICAL, PHYSICAL & ENGINEERING SCIENCES

Table 1

$HgI_2(X^1\Sigma_g^+)$	ν/cm^{-1}
Q_s (symmetric stretch)	155[a]
Q_a (antisymmetric stretch)	237[b]
q (bend)	33[c]
D (dissociation energy)/cm^{-1}	21000[d]
$HgI(X^2\Sigma^+)$[e]	
ω_e/cm^{-1}[f]	125
D/cm^{-1}	2800
β ($\beta^2 = \omega_e^2/4B_e$)	7.1
r_e/Å	2.80
$HgI(B^2\Sigma^+)$[e]	
ω_e/cm^{-1}[f]	110
D/cm^{-1}	18850
β	2.9
r_e/Å	3.30

$HgI(B^2\Sigma^+ \leftarrow X^2\Sigma^+)$ transition dipole: $\mu = 4\exp[-(r-3.39)^2/0.9^2]$ debye[g]

potential parameters	PES (*a*)	PES (*b*)
D_0/cm^{-1}	2800	2800
D_1/cm^{-1}	−1000	−1000
σ_D/Å	1	1
β_0	7.1	7.1
β_1	0.5	5.5
σ_β/Å	0.50	0.75
$\sigma_{\beta+}$/Å	2.5	2.5
r_{e0}/Å	2.8	2.8
r_{e1}/Å	0.4	0.2
σ_r/Å	1.5	1.0
$\gamma/Å^{-1}$	1.5	2.3

[a] Value taken from Klemperer (1956).
[b] Value taken from Braune & Engelbrecht (1932).
[c] Value taken from Sponer & Teller (1941).
[d] Value taken from Hofmann & Leone (1978).
[e] Values taken from Wieland (1929).
[f] Values of D, β and r_e were chosen so as to yield the optimum overall representation of the ground-state potential energy function and the best representation of the accessed vibrational levels of the excited state.
[g] Based on figure 3 of McGarvey *et al.* (1981). 1 debye $\approx 2.7 \times 10^{-29}$ Cm.

D_0, β_0 and r_{e0} are fixed to give a 'best fit' Morse potential for the $X^2\Sigma^+$ state of HgI at large separations. The resulting surface is very flexible near the transition state. For small β_1 and γ, a wide-channel surface results, while for large β_1 and γ, a narrow channel surface results. We have chosen two surfaces for study, shown in figure 4. The wide-channel surface (*a*) corresponds to that used in the classical trajectory simulations (Dantus *et al.* 1989*b*). The numerical parameters used (as well as other parameters relating to the ground states of HgI_2, the $X^2\Sigma^+$ and $B^2\Sigma^+$ states of HgI and dipole moment functions) are summarized in table 1.

For simplicity, and to allow better comparison with the classical trajectory study the same surface (either (*a*) or (*b*)) is used for both the I and I* channels, with different excess energies to simulate the spin–orbit splitting of 7600 cm^{-1}. While the repulsive walls could be further adjusted to give better agreement with experimental absorption cross-sections, this still yields results in fair accord with the photolysis

PHILOSOPHICAL TRANSACTIONS OF THE ROYAL SOCIETY A MATHEMATICAL, PHYSICAL & ENGINEERING SCIENCES

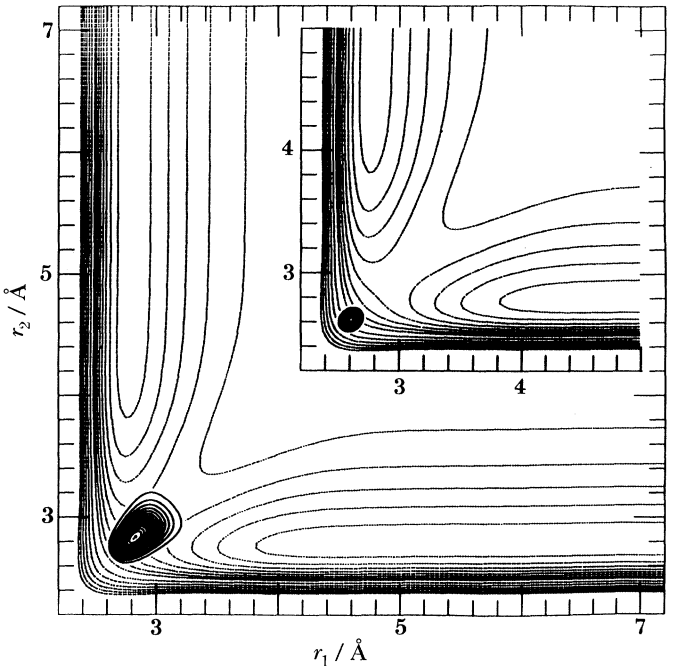

Figure 5. Pumping the ground-state wave packet (insert) to 1000 cm^{-1} above total dissociation (Hg + 2I) in the I* channel results in translation of the wave packet along the symmetric stretching coordinate, as well as broadening, mostly in the same direction. However, the most important features of the early-time behaviour (less than a few vibrational periods) can be obtained by the 'shifted δ-function pulse' approximation, using as an initial wave packet the ground-state wave function shifted along the symmetric coordinate to achieve energy conservation.

experiments of Hofmann & Leone (1978) and has relatively little effect on the simulation of presently available FTS results (Bowman *et al.* 1989*b*; Dantus *et al.* 1989*b*). Given the model nature of the problem, more detail is not warranted until good *ab initio* surfaces become available.

(*b*) *Wave packet motion*

In this section, we first consider 'pumping' of the ground state wave packet to the dissociative reaction surface, and then present the results of calculations on surfaces (*a*) and (*b*). In the asymptotic limit, slices perpendicular to the translational coordinate r_1 are used to characterize vibrational coherence and populations.

As an example of a laser-pump simulation, figure 5 shows the result of a 310 nm pulse with $\sigma_t = 70$ fs exciting the $v'' = 0$ ground state of HgI_2 to the I* surface. In this particular calculation, the parameters of surface (*b*) have been slightly varied to bring the absorption cross section into agreement with the experimental values of Hofmann & Leone (1978). The main effect of the finite pump pulse is to broaden somewhat the wave packet and to shift it along the symmetric stretching coordinate, particularly in the off-resonant case, where the shift and broadening achieve energy conservation to within the laser spectral width.

We find (as for other systems such as I_2 or NaI) that for a few vibrational periods, this effect can be mimicked fairly closely by a 'shifted δ-function pulse', in which the ground-state wave function is shifted along the direction of steepest descent until its energy expectation value satisfies energy conservation within the laser bandwidth.

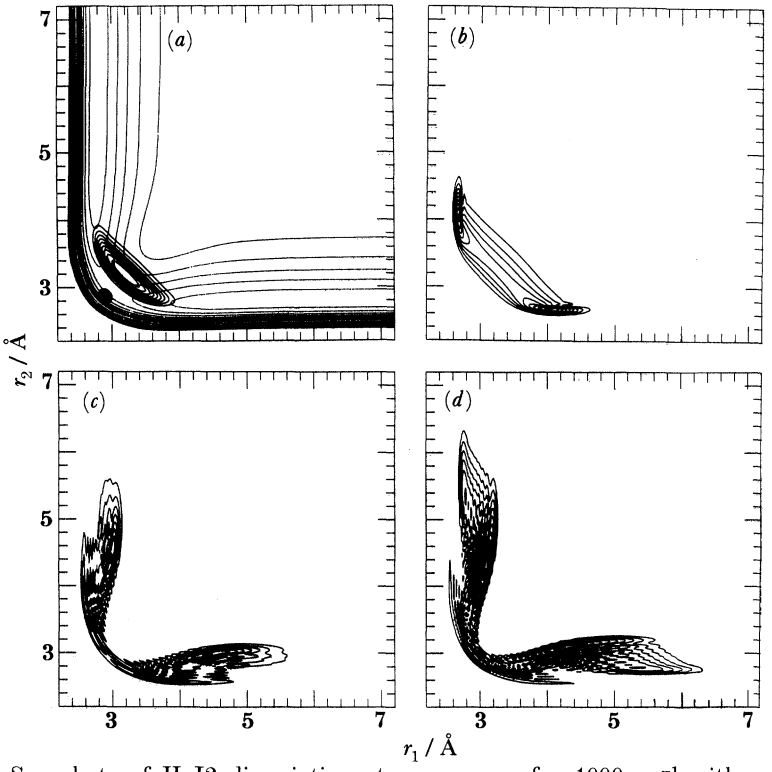

Figure 6. Snapshots of HgI2 dissociation at an energy of $-1000\ \mathrm{cm^{-1}}$ with respect to total dissociation on surface (*b*): the narrow-channel surface effectively funnels the wave packet into the asymptotic region, resulting in low vibrational excitation compared to a similar calculation on surface (*a*) (see figure 10*a*). (*a*) 155 fs, (*b*) 233 fs, (*c*) 389 fs, (*d*) 467 fs.

The main error introduced by use of the 'shifted δ-function pulse' is an increase in the complexity of the long-time dynamics arising from an energy spread of the wave packet that may be greater than the laser spectral width. To facilitate comparison with classical trajectory studies, where gaussian Monte-Carlo distributions of uniform width were used, this is the procedure we adopt in the following with the initial wavefunctions on the dissociative surface.

Wave packet propagations were done at -1000, 1350 and 8950 $\mathrm{cm^{-1}}$ on surfaces (*a*) and (*b*). Figures 6–8 show some examples of HgI_2 dissociation at different excess energies. Figure 6 corresponds to an energy of about $-1000\ \mathrm{cm^{-1}}$ with respect to the full (Hg+2I) dissociation limit on surface (*b*). The narrow-channel surface confines the dissociating wave packet, which essentially flows along equipotential contours. Figure 7 corresponds to an energy of 1350 $\mathrm{cm^{-1}}$ on surface (*a*), and represents the simplest picture of I* channel dissociation. Here, there is considerably more motion in the symmetric coordinate, until the expanding wave packet diffuses back into the walls of the HgI potential well at $t > 300$ fs. At 800 fs, well-developed 'clouds' of Hg+I, I+HgI, and I+Hg+I have formed. The early-time symmetric stretching behaviour becomes even more dramatic in the case of *ca.* 8950 $\mathrm{cm^{-1}}$ excitation energy on surface (*b*), corresponding to the simplest picture of I channel dissociation. The wave packet proceeds along the symmetric coordinate over a distance of 5 Å before beginning to separate into three sections. Clearly, the most important motions

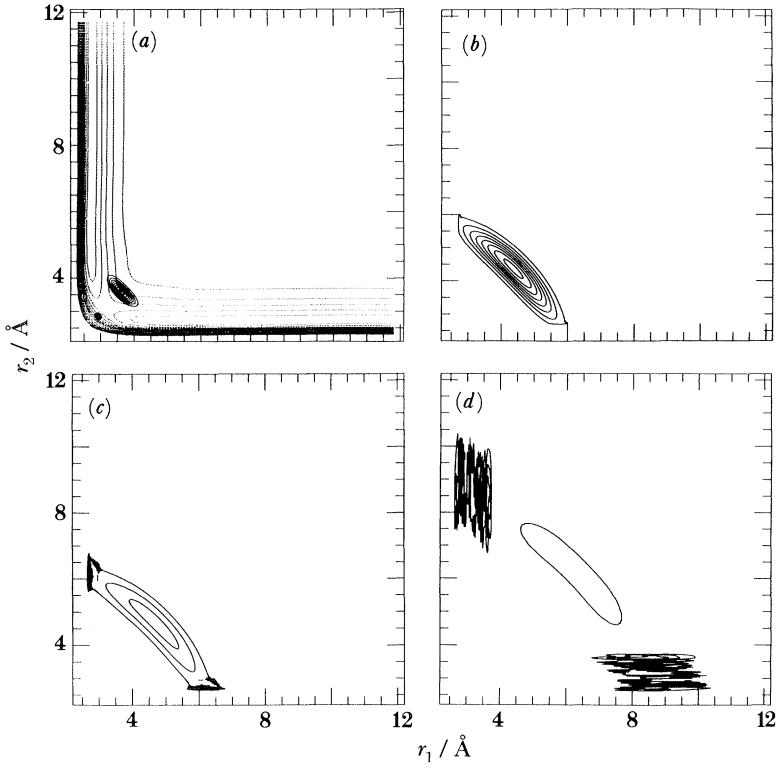

Figure 7. HgI_2 wave packet at 1350 cm^{-1} on surface (*b*), corresponding to I* channel dissociation. At early times, motion is predominantly along the symmetric stretch, until diffusion into the wells occurs, and the wave packet separates into three fragments for HgI + I, I + HgI and I + Hg + I. (*a*) 160 fs, (*b*) 320 fs, (*c*) 400 fs, (*d*) 800 fs.

during the initial phase of the dissociation reaction are not required to be along the natural reaction coordinate (path of steepest descent leading to products) in the present case. While at low energies the steepest descent path is good for parametrization of the reaction, at higher energies, motion proceeds along it only at very early times (symmetric coordinate) and very long times (along r_1). Finally, the three energies correspond to total dissociation (mercury and two iodines) of approximately 0, 25 and 90% on surface (*a*), and 0, 20 and 80% on surface (*b*).

In the asymptotic limit, one can obtain approximate vibrational product distributions by taking sections of the wave packet perpendicular to the translational coordinate r_1, projecting onto the $HgI(X^2\Sigma^+)$ bound eigenstates (equation (11)), and summing the weighted distributions of all sections at different r_1 to obtain a translationally averaged vibrational distribution (with all coherent effects averaged out). Generally, the average vibrational quantum number decreases with increasing r_1 of the sections, as shown in figure 9 for the wave packet from figure 6 at $t = 467$ fs. One would expect so at long times, when the translationally fastest part of the wave packet should have the smallest vibrational excitation, and vice versa. This is not necessarily the case for short times even in the asymptotic region (greater than 4.5 Å), when the wave packet still undergoes complicated non-separable motions in the two coordinates. The approximate monotonicity of the vibrational distribution as a function of r_1 is a prerequisite for the application of the sectioning method.

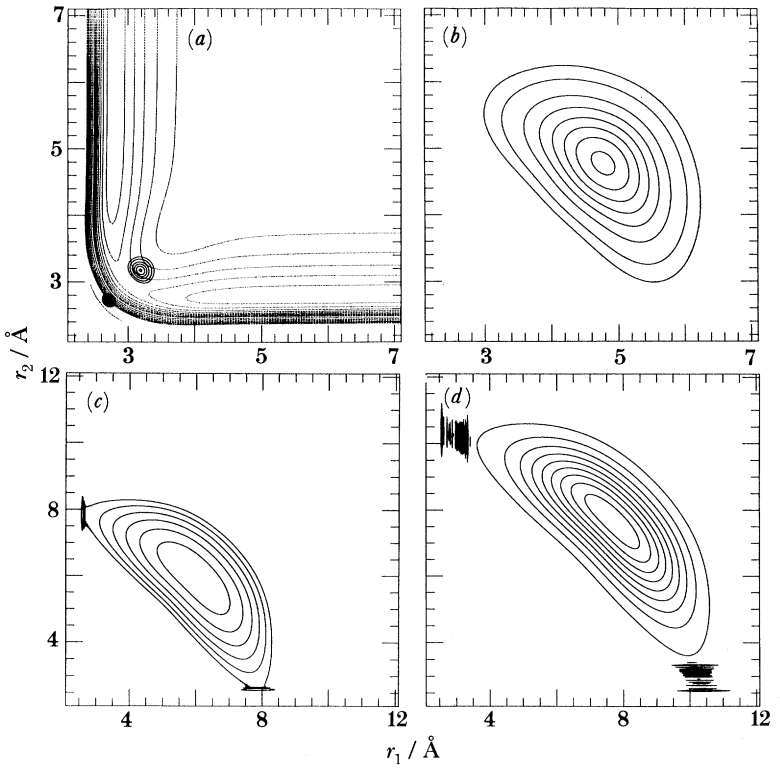

Figure 8. At 8950 cm^{-1} of excess energy (I channel), the symmetric motion persists up to 250 fs and 5 Å for the packet centroid, before vibrational structure appears in the wings of the wave packet. (*a*) 58 fs, (*b*) 233 fs, (*c*) 400 fs, (*d*) 600 fs.

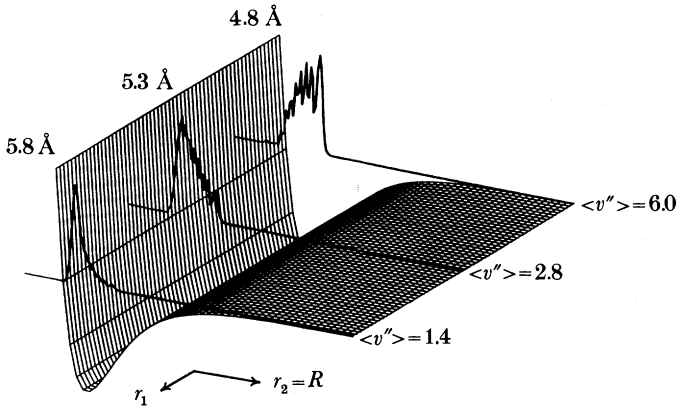

Figure 9. Slices at three distances along the dissociation coordinate r_1 through the asymptotic region of the wave packet of figure 6 at 467 fs. Translational diffusion has sorted the vibrational excitation such that by energy conservation, the slowest HgI molecules have the highest vibrational excitation, while the fastest molecules have low vibrational excitation. The slices shown are $\Sigma|\Psi_i(R)\rangle\langle\Psi(r_1 = \text{const.}, r_2 = R, t)|\Psi_i(R)\rangle|^2$.

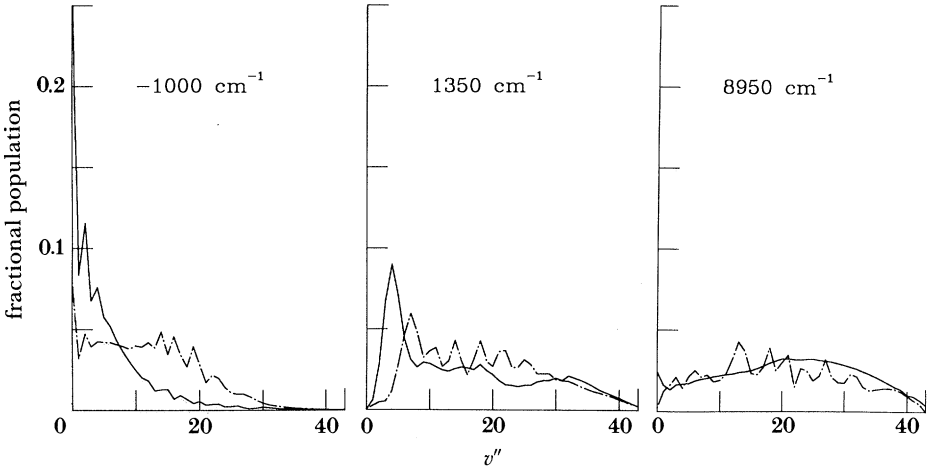

Figure 10. Vibrational distributions for PES (*a*) (dotted) and PES (*b*) (solid); the narrow-channel PES leads to lower vibrational excitation, which is in somewhat better agreement with experimental observations. As expected, higher energies lead to wider distributions with higher average v.

Figure 10 shows asymptotic vibrational distributions for potentials (*a*) and (*b*) at the three energies studied. The wider-channel PES generally causes a marked increase in the vibrational excitation. This is to be expected, since it results in wider ranging initial motion along the symmetric coordinate, which is partially transferred into a larger vibrational amplitude. This is also reflected in the higher total dissociation yields on surface (*a*). On both surfaces, as the excess energy is increased, the vibrational distribution broadens considerably and moves to higher average v''.

(*c*) *Comparison with experiment*

We now derive from the above observations several quantities, such as emission spectra of the probed HgI, and oscillatory effects in the transients due to wave packet motion, which can be more directly compared with experiment, and conclude with a comparison with previous classical results. This suggests several avenues for further study.

The simplest parameter for comparison is the reaction time. A long-lived transition state would be reflected in a delay of the experimental transient rise time. At 310 nm, less than 500 fs delays were observed in the I and I* channels (Bowman *et al.* 1989*b*; Dantus *et al.* 1989*b*), with prompt (*ca.* 100 fs) appearance of a full Hg+2I dissociation peak in the former, and regular vibrational motion following a short induction period (*ca.* 300 fs) on the non-asymptotic part of the PES for the latter. (An accurate $t = 0$ measurement has not been made yet.) In our calculations, the I-channel wave packets reach the asymptotic (greater than 4.5 Å) region in about 200 fs, while the I*-channel packet requires about 350 fs, comparing well with the experimental times for a prompt reaction. Even at -1000 cm^{-1} energy, no 'full' resonance effects were observed near the transition state in the wave packet motion.

While the small r_1 behaviour of the surface connecting to $B^2\Sigma^+$ is not known, some deductions can be made about the early-time transients in figure 2 based on figures 7 and 8. Both the I and I* channel packets initially move along the symmetric coordinate, although the I channel packet does so faster and loses less amplitude into the HgI well (corresponding to its much higher fractional dissociation). The strong

PHILOSOPHICAL TRANSACTIONS OF THE ROYAL SOCIETY A MATHEMATICAL, PHYSICAL & ENGINEERING SCIENCES

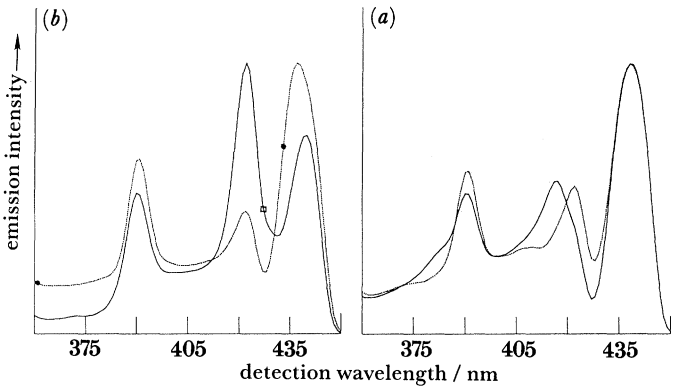

Figure 11. Emission spectra calculated from the vibrational distributions in figure 10. For surface (*b*), black circles indicate 360 and 432.5 nm detection, where the I channel (– – –) is more prevalent, while the square indicates 427.5 nm, where the I* (—) channel dominates. At 440 nm, the two are comparable. The emission spectra have not been scaled for the combined effects of total dissociation and pump cross-section.

first peak of the I transient (figure 2*c*) and the 'truncated' peak of the I* transient (figure 2*b*) probed at $\lambda_2 = 390$ nm are likely due to an absorption process near the end of that symmetric motion part of the wave packet motion. The short initial period in the transient detected at $\lambda_{det} = 440$ nm and probed at the same wavelength (Dantus *et al.* 1989*b*) is then mostly due to a signal from the I-channel wave packet moving along the symmetric stretching coordinate. At even earlier times, the transients probed at $\lambda_2 = 620$ nm (figure 2*a*) result from first the I channel, and then the I*-channel wave packets moving out along the symmetric coordinate and through a resonance absorption region. If one could assume that both the reactive surfaces (giving rise to $HgI(X^2\Sigma^+)$) and final probe surfaces (leading to $HgI(B^2\Sigma^+)$) were pairwise shifted copies (as we assumed for the reactive surface calculations; see §4(*a*), the delay between peaks in figure 2*a* would be a direct reflection of the kinetic energy difference between the two channels; the unknown characteristics of the PESS (particularly for the upper surfaces) may introduce an additional resonance absorption related shift. This is supported by figures 7 and 8, which indicate a shift of *ca.* 100 fs, whereas the experiments yield a shift of 200 fs. Measurements at more pump energies will allow a spectral/temporal mapping of the reactive and probe PESS near the transition state and reveal further information about their detailed nature.

As can be seen from figure 3, the vibrational product distributions presented in the previous section manifest themselves in the energy-resolved emission spectra. Figure 11*a*, *b* shows emission spectra resulting from near-asymptotic wave packets (greater than 4.5 Å) on surfaces (*a*) and (*b*) at 1350 and 8950 cm^{-1} corresponding to the I* and I channels. The emission spectra have not been scaled for photolysis yield (3.7:1, I:I* at 310 nm, Hofmann & Leone 1978) and total dissociation. For surface (*b*), the two effects cancel, and figure 11*a* directly shows in which regions either channel is dominant; for surface (*a*), the I* emission should be multiplied by about 2. For either PES (particularly (*b*)), the I and I* channel intensities vary sufficiently to allow selection of specific surface dynamics. As observed experimentally (Bowman *et al.* 1989*b*; Dantus *et al.* 1989*b*), transient detection at 360 and 432.5 nm is more sensitive to the I channel, while detection at 427.5 nm is more sensitive to the I* channel, and detection at 440 nm is about equally sensitive to both. The product state

PHILOSOPHICAL TRANSACTIONS OF THE ROYAL SOCIETY A MATHEMATICAL, PHYSICAL & ENGINEERING SCIENCES

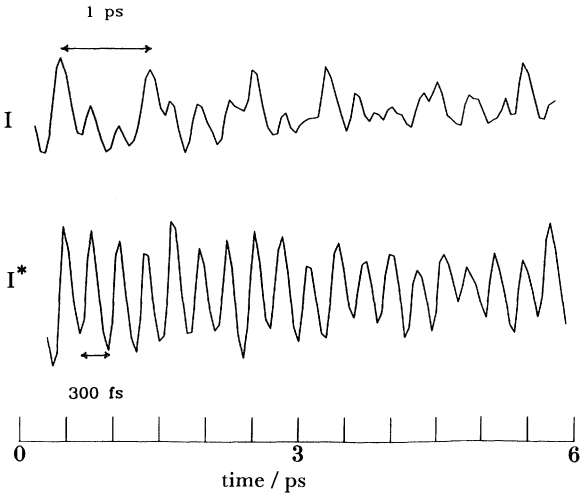

Figure 12. $\lambda_2 = 390$ nm FTS transients from the wave packets on surface (*b*) for the I and I* channels. The vibrational periods are in close agreement with experiment, although the transients are more structured due to a total LIF simulation (no monochromator) and absence of smoothing due to imperfect pulse cross-correlations. The calculations do not start at $t = 0$ since the section approximation was made, which is valid only after about 300 fs.

distributions for the 'tight' surface (*b*) on the whole agree better with the experimental findings than those of the wide-channel surface, mainly due to the lower vibrational excitation in the I* channel.

Using the sectioning approximation at $t > 300$ fs and $X^2\Sigma^+ - B^2\Sigma^+$ Franck–Condon factors, we can calculate FTS transients using equation (11), maintaining the complex expansion coefficients of $\Psi(t)$ in terms of bound states to extract the coherence effects, and summing over sections weighted by their amplitude. Figure 12 shows FTS transients for the I and I* channels on surface (*b*), calculated for a probe wavelength of 390 nm. The periods correspond closely to the experimental observations. Two features deserve special mention. Because the calculated transients correspond to detection of all the LIF signal (rather than $\lambda_{det} \pm 5$ nm as in the experiments), and are not convoluted with a 'monochromator' response function, they show more structure than experimentally observed; it is also notable that even the fairly broad vibrational distribution at 8950 cm^{-1} on surface (*b*) (figure 10) yields sharp, well defined FTS maxima with a 1 ps period. The width of the distribution does lead to some irregularities in the period at longer times; indeed some weak features have been observed (Dantus *et al.* 1989*b*) in the experimental transients (see figure 2*c*) which may correspond to this more complex behaviour. Surface (*a*) yields similar FTS spectra.

As befits the heaviness of the Hg and I atoms, the dissociation times from the quantum and classical simulations are in good agreement (*ca.* 200 fs in the I channel, *ca.* 350 fs in the I* channel), indicating a prompt dissociation as observed experimentally (Bowman *et al.* 1989*b*; Dantus *et al.* 1989*b*). The most prominent difference between the quantum and classical (Dantus *et al.* 1989*b*) calculations is the higher total dissociation yield via both channels in the quantum simulations. This may to some extent be due to the large energy spread in the 'shifted δ-pulse' gaussian wave packet, which amounts to 500 rather than 200 cm^{-1}. The quantum simulations

show more clearly the importance of symmetric motion at early times compared with the classical calculations, which are fully confined by even the shallow outer walls of the potential well (cf. fig. 13 of Dantus *et al.* 1989*b*). Hence surface (*b*) is slightly more preferable in the quantum calculations, while satisfactory results were obtained from surface (*a*) in the classical simulations. However, it should be emphasized that these slight variations do not imply fundamental differences between classical and quantum results. Experiments at lower energies should indicate the presence or absence of resonances, and thus establish the nature of the force field at the transition state directly.

5. Conclusions

The wave packet motions at the I and I* channel energies allow a pictorial understanding of the FTS observations. The early time (0–200 fs) transients arise from wave packets moving along the symmetric stretching coordinate towards total dissociation. At slightly longer times (200–500 fs), diffusion into the potential wells sets in, and the vibrational motion of the wave packets translates into oscillations of the FTS signal. Both classical and quantum calculations produce results that are tantalizingly close to experimental observations (Bowman *et al.* 1989*b*; Dantus *et al.* 1989*b*), but the case of the HgI_2 dissociation reaction is clearly still far from closed. Experiments at longer pump wavelengths ($310 < \lambda < 330$ nm) will be able to probe sensitively the region near the transition state in the I* channel; at even longer wavelengths, the I channel may reveal a PES considerably different from the I* surface. Careful alignment studies at several excitation energies should allow experiments to pinpoint the location of surface crossings and the role of the bending vibration in the reaction. As evident from figure 10, product state distributions can also yield valuable information on the reaction.

In parallel, *ab initio* surfaces of the transition state region would be very desirable as a basis for further quantum and classical theoretical studies. In particular, three-dimensional studies, including the bending motion and HgI in-plane rotation will then become useful in interpreting the longer-time behaviour of the FTS signal, and finer details of the short-time signal.

This work was supported by the U.S. Air Force Office of Scientific Research under grant number AFOSR 90-0014. We are grateful to Professor R. A. Marcus for his helpful comments. One of us (G. R.) thanks SERC for the award of a NATO Postdoctoral Fellowship. Some of the calculations reported in this paper were carried out on the Cray X-MP/18 supercomputing at the Jet Propulsion Laboratory.

References

Allen, P. W. & Sutton, L. E. 1950 *Acta Cryst.* **3**, 46.
Benjamin, I. & Wilson, K. R. 1989 *J. chem. Phys.* **90**, 4176.
Bernstein, R. B. & Zewail, A. H. 1989 *J. chem. Phys.* **90**, 829.
Bersohn, R. & Zewail, A. H. 1988 *Ber. Bunsenges. phys. Chem.* **92**, 373.
Bhartiya, J. B., Behere, S. H. & Rao, M. L. P. 1990 *J. quant. Spectrosc. radiat. Transfer* **43**, 95.
Bowman, R. M., Dantus, M. & Zewail, A. H. 1989*a* *Chem. Phys. Lett.* **161**, 297.
Bowman, R. M., Dantus, M. & Zewail, A. H. 1989*b* *Chem. Phys. Lett.* **156**, 131.
Braune, H. & Engelbrecht, G. 1932 *Z. phys. chem.* B**19**, 303.
Butkow, K. 1931 *Z. Phys.* **71**, 678.
Cheung, N.-H. & Cool, T. A. 1979 *J. quant. Spectrosc. radiat. Transfer* **21**, 397.
Cheung, N.-H., McGarvey Jr., J. A., Erlandson, A. C. & Cool, T. A. 1982 *J. chem. Phys.* **77**, 5467.

PHILOSOPHICAL TRANSACTIONS OF THE ROYAL SOCIETY A MATHEMATICAL, PHYSICAL & ENGINEERING SCIENCES

Choi, S. E. & Light, J. C. 1989 *J. chem. Phys.* **90**, 2543.
Dantus, M., Rosker, M. J. & Zewail, A. H. 1987 *J. chem. Phys.* **87**, 2395.
Dantus, M., Rosker, M. J. & Zewail, A. H. 1988 *J. chem. Phys.* **89**, 6128.
Dantus, M., Bowman, R. M., Baskin, J. S. & Zewail, A. H. 1989*a* *Chem. Phys. Lett.* **159**, 406.
Dantus, M., Bowman, R. M., Gruebele, M. & Zewail, A. H. 1989*b* *J. chem. Phys.* **91**, 7437.
Dantus, M., Bowman, R. M. & Zewail, A. H. 1990 *Nature, Lond.* **343**, 737.
Dreiling, T. D. & Setser, D. W. 1983 *J. chem. Phys.* **79**, 5423.
Engel, V. & Metiu, H. 1989*a* *J. chem. Phys.* **90**, 6116.
Engel, V. & Metiu, H. 1989*b* *J. chem. Phys.* **91**, 1596.
Engel, V. & Metiu, H. 1989*c* *Chem. Phys. Lett.* **155**, 77.
Engel, V. & Metiu, H. 1990 *J. chem. Phys.* **92**, 2317.
Engel, V., Metiu, H., Almeida, R., Marcus, R. A. & Zewail, A. H. 1988 *Chem. Phys. Lett.* **152**, 1.
Engel, V., Schinke, R., Hennig, S. & Metiu, H. 1990 *J. chem. Phys.* **92**, 1.
Feit, M. D. & Fleck Jr., J. A. 1983 *J. chem. Phys.* **78**, 301.
Feit, M. D., Fleck Jr., J. A. & Steiger, A. 1982 *J. comp. Phys.* **47**, 412.
Fleck Jr., J. A., Morris, J. R. & Feit, M. D. 1976 *Appl. Phys.* **10**, 129.
Gruebele, M., Roberts, G., Dantus, M., Bowman, R. M. & Zewail, A. H. 1990 *Chem. Phys. Lett.* **166**, 459.
Gruebele, M. & Zewail, A. H. 1990 *Physics Today* **43** (5), 24.
Heather, R. & Metiu, H. 1989 *Chem. Phys. Lett.* **157**, 505.
Heller, E. J. 1975 *J. chem. Phys.* **62**, 1544.
Heller, E. J. 1981 *Acct. chem. Res.* **14**, 368.
Henriksen, N. E. & Heller, E. J. 1989 *J. chem. Phys.* **91**, 4700.
Hofmann, H. & Leone, S. R. 1978 *J. chem. Phys.* **69**, 3819.
Huber, D. & Heller, E. J. 1987 *J. chem. Phys.* **87**, 5302.
Husain, J., Wiesenfeld, J. R. & Zare, R. N. 1980 *J. chem. Phys.* **72**, 2479.
Hutchinson, M. H. R. & Theocharous, E. S. 1981 *Chem. Phys. Lett.* **81**, 553.
Imre, D. G. & Zhang, J. 1989 *Chem. Phys.* **139**, 89.
Johnson, B. R. 1977 *J. chem. Phys.* **67**, 4086.
Khundkar, L. R. & Zewail, A. H. 1990 *A. Rev. phys. Chem.* (Submitted.)
Klemperer, W. 1956 *J. chem. Phys.* **25**, 1066.
Kono, H. & Fujimura, Y. 1989 *J. chem. Phys.* **91**, 5860.
Kosloff, R. 1988 *J. phys. Chem.* **92**, 2087.
Kosloff, D. & Kosloff, R. 1983*a* *J. comp. Phys.* **52**, 35.
Kosloff, R. & Kosloff, D. 1983*b* *J. chem. Phys.* **79**, 1823.
Lee, S.-Y., Pollard, W. T. & Mathies, R. A. 1989*a* *J. chem. Phys.* **90**, 6146.
Lee, S.-Y., Pollard, W. T. & Mathies, R. A. 1989*b* *Chem. Phys. Lett.* **160**, 531.
Lee, S.-Y., Pollard, W. T. & Mathies, R. A. 1989*c* *Chem. Phys. Lett.* **163**, 11.
Lin, S. H. & Fain, B. 1989 *Chem. Phys. Lett.* **155**, 216.
Loudon, R. 1973 *The quantum theory of light*. Oxford: Clarendon Press. (338 pages.)
Marcus, R. A. 1988 *Chem. Phys. Lett.* **152**, 8.
Maya, J. 1977 *J. chem. Phys.* **67**, 4976.
Maya, J. 1978 *Appl. Phys. Lett.* **32**, 484.
Mayer, T. M., Wilcomb, B. E. & Bernstein, R. B. 1977*a* *J. chem. Phys.* **67**, 3507.
Mayer, T. M., Muckerman, J. T., Wilcomb, B. E. & Bernstein, R. B. 1977*b* *J. chem. Phys.* **67**, 3522.
McGarvey Jr, J. A., Cheung, N.-H., Erlandson, A. C. & Cool, T. A. 1981 *J. chem. Phys.* **74**, 5133.
Oprysko, M. M., Aoiz, F. J., McMahan, M. A. & Bernstein, R. B. 1983 *J. chem. Phys.* **78**, 3816.
Rose, T. S., Rosker, M. J. & Zewail, A. H. 1988 *J. chem. Phys.* **88**, 6672.

PHILOSOPHICAL TRANSACTIONS OF THE ROYAL SOCIETY A MATHEMATICAL, PHYSICAL & ENGINEERING SCIENCES

Rose, T. S., Rosker, M. J. & Zewail, A. H. 1989 *J. chem. Phys.* **91**, 7415.
Rosker, M. J., Rose, T. S. & Zewail, A. H. 1988*a* *Chem. Phys. Lett.* **146**, 175.
Rosker, M. J., Dantus, M. & Zewail, A. H. 1988*b* *J. chem. Phys.* **89**, 6113.
Salter, C., Tellinghuisen, P. C., Ashmore, J. G. & Tellinghuisen, J. 1986 *J. molec. Spectrosc.* **120**, 334.
Scherer, N. F., Knee, J. L., Smith, D. D. & Zewail, A. H. 1985 *J. chem. Phys.* **89**, 5141.
Sponer, H. & Teller, E. 1941 *Rev. Mod. Phys.* **13**, 75.
Tellinghuisen, J., Tellinghuisen, P. C., Davies, S. A., Berwanger, P. & Viswanathan, K. S. 1982 *Appl. Phys. Lett.* **41**, 789.
Terenin, A. 1927 *Z. Phys.* **44**, 713.
Viswanathan, K. S. & Tellinghuisen, J. 1983 *J. molec. Spectrosc.* **98**, 185.
Wadt, W. R. 1979 *Appl. Phys. Lett.* **34**, 658.
Wadt, W. R. 1980 *J. chem. Phys.* **72**, 2469.
Wehrli, M. 1938 *Helv. phys. Acta* **11**, 339.
Wehrli, M. 1940 *Helv. phys. Acta* **13**, 153.
Whitehurst, C. & King, T. A. 1987 *J. Phys.* B: *Atom. Molec. Phys.* **20**, 4053.
Wieland, K. 1929 *Helv. phys. Acta* **2**, 46.
Wieland, K. 1932 *Z. Phys.* **76**, 801.
Wieland, K. 1960 *Z. Elektrochem.* **64**, 761.
Wilcomb, B. E. & Bernstein, R. B. 1976 *J. molec. Spectrosc.* **62**, 442.
Wilcomb, B. E., Mayer, T. M., Bernstein, R. B. & Bickes Jr, R. W. 1976*a* *J. Am. chem. Soc.* **98**, 4676.
Wilcomb, B. E., Haberman, J. A., Bickes Jr, R. W., Mayer, T. M. & Bernstein, R. B. 1976*b* *J. chem. Phys.* **64**, 3501.
Wilcomb, B. E., Burnham, R. & Djeu, N. 1980 *Chem. Phys. Lett.* **75**, 239.
Williams, S. O. & Imre, D. G. 1988*a* *J. phys. Chem.* **92**, 6636.
Williams, S. O. & Imre, D. G. 1988*b* *J. phys. Chem.* **92**, 6648.
Yamashita, K. & Morokuma, K. 1989 *J. chem. Phys.* **91**, 7477.
Yan, Y.-J., Fried, L. E. & Mukamel, S. 1989 *J. phys. Chem.* **93**, 8149.
Zewail, A. H. 1988 *Science, Wash.* **242**, 1645.
Zewail, A. H. 1989 *J. chem. Soc. Faraday Trans.* II **85**, 1221.
Zewail, A. H. & Bernstein, R. B. 1988 *Chem. Engng News.* **66**, 24.
Zhang, F. M., Oba, D. & Setser, D. W. 1987 *J. phys. Chem.* **91**, 1099.

PHILOSOPHICAL TRANSACTIONS OF THE ROYAL SOCIETY A MATHEMATICAL, PHYSICAL & ENGINEERING SCIENCES